Protein Pre-Binding State (PBS) Framework Enables Mechanistic Insights and Engineering of Robust Biocatalysts for Plastic Depolymerization

Xiaoyu Zhang, Kele Zhang, Nayifan Luo, Zicong Chen, Xuanqi Ni, Guangyu Liu, Chen Chen, Xinglin Yu, Zongling Yu, Wenjie Zhai, Yueyang Du, Zimo Jiang, Chuai Rao, Yunhong Zhang, Yihao Tao, Lezi Xue, Jiayi Li

Abstract

Biotechnological recycling offers a sustainable solution to plastic pollution, with polyethylene terephthalate (PET) posing the most urgent challenge. Rapid PET depolymerization requires robust biocatalysts. We introduce a protein pre-binding state (PBS) framework that captures transition-state–like conformations crucial for catalysis, enabling efficient identification of reactive geometries without exhaustive QM/MM sampling. Guided by PBS, we engineered leaf and branch compost cutinase (LCC), achieving three rounds of improvement. The resulting variant, LCC-ICCG-R2, depolymerized more than 90% of pretreated post-consumer PET at 75 °C within 4 h, yielding over 92% terminal products. Extending PBS beyond PET, we designed a bio-based pyrrolidone-containing polyester (PBTDP) that undergoes efficient enzymatic depolymerization under mild conditions. These applications establish PBS as a versatile platform bridging mechanistic understanding with practical advances in sustainable polymer recycling and computational enzyme design.

1. Introduction

There is an urgent need for circular recycling routes for commodity plastics. Owing to the limited availability of sustainable end-of-life treatments and persistently low recycling rates, plastic pollution has escalated into a worldwide environmental crisis, posing significant risks to ecosystem (1–3). Developing circular recycling routes is therefore of urgent importance (4,5). Among plastics, poly(ethylene terephthalate) (PET) is particularly critical due to its global prevalence in packaging and textiles. Its durability and moisture resistance, though valuable in use, have driven large-scale accumulation of PET waste in the environment (6,7). Current recycling strategies for PET include mechanical, chemical, and biological approaches. Enzymatic hydrolysis has attracted growing attention because of its potential for closed-loop monomer recovery. Significant efforts have led to the discovery, engineering, and evolution of PET-active hydrolases with improved activity, stability, and substrate tolerance (8,9). Notably, the thermostable cutinase variant LCC-ICCG operates optimally at 65 °C and achieves substrate conversions of ≥90% at high substrate loadings, thereby underscoring its potential for industrial application. In contrast, other hydrolases such as HotPETase and FATS-PETase show considerably lower efficiencies under similar conditions (10).

At the molecular level, PET hydrolysis occurs at bio-environmental interfaces where localized physicochemical conditions dictate substrate binding and enzymatic activity (11,12). Unlike soluble small molecules, PET presents a rigid, hydrophobic, and often crystalline surface that restricts access to ester bonds, making catalysis highly dependent on enzyme–substrate recognition and interfacial dynamics (13,14). Computational methods such as MD simultaions and QM/MM simulations have provided valuable atomistic insights into these processes. However, a systematic framework that integrates computational exploration with directed enzyme remodeling remains lacking (15).

Here, we propose a computationally guided strategy termed PBS, which leverages near-attack state analysis to rationalize and enhance PET hydrolase performance. PBS comprises four modules:mutation, docking, kinetic simulation, and evaluation, designed to map enzyme–substrate compatibility and streamline mutant screening. Using PBS, we first confirmed that LCC-ICCG possesses significantly higher catalytic efficiency than other PET hydrolases, providing clear evidence of its advantages for enzymatic polyester depolymerization, applying the platform to engineer improved ICCG variants. The optimized variant, obtained through iterative design and directed evolution, was able to depolymerize more than 91% of pretreated post-consumer PET within just 4 hours. This work not only advances mechanistic understanding of enzyme–polymer interactions but also provides a scalable strategy for designing high-performance biocatalysts with direct relevance to global sustainability challenges.

2. Results

2.1 Computational Framework Based on the Pre-Binding State (PBS)

We developed the Pre-Binding State (PBS) model to integrate mechanistic principles from both Houk's transition-state (TS) theory and Warshel's binding–entropy perspective. In this framework,

catalytically relevant conformations preceding the TS were sampled from molecular dynamics (MD) trajectories and evaluated using MM/GBSA energies and root-mean-square deviations (RMSD). This allowed direct assessment of the effects of amino acid substitutions on substrate recognition, reactivity, and mutational fitness. Variants predicted to destabilize the rate-determining TS analog were excluded, while favorable conformations were ranked by electrostatic stabilization of the TS.

The PBS descriptors exhibited strong stereoelectronic interpretability. By mapping energetic parameters onto conformational populations, we constructed catalytically competent states that rationalize reduced activation enthalpy and improved transition-state stabilization. This framework thereby bridges chemical theory with enzyme design and provides a predictive basis for variant selection (Figure 1).
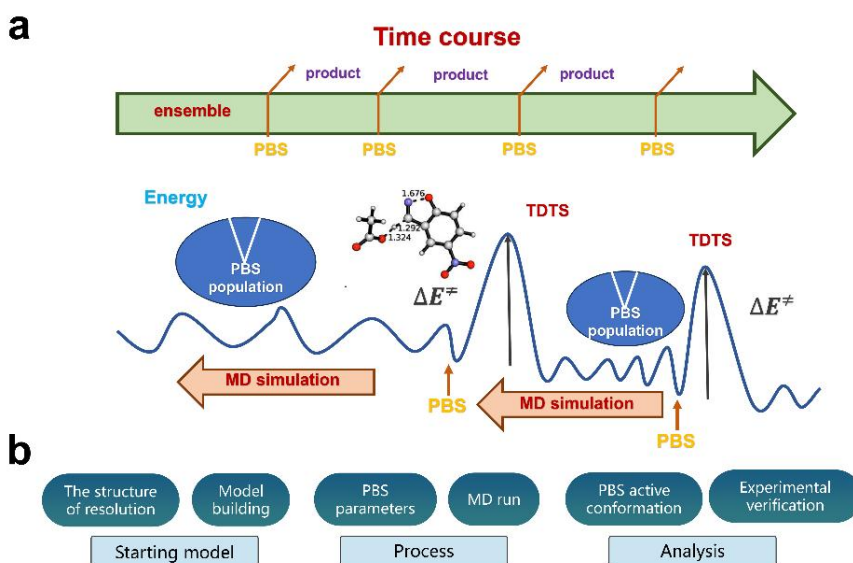

Figure 1: Design strategies based on the PBS. (a) Schematic of the "PBS" parameter model in the Michaelis-Menten model of an enzyme-catalyzed reaction. (b) The steps consisted of three main phases.

2.2 Favorable PBS Conformations Facilitate PET Hydrolysis by LCC-ICCG

PETase follow the canonical two-step catalytic pathway characteristic of cutinases (Scheme 1) (16). The process begins with an acylation step, during which a covalent acylenzyme intermediate is formed and a hydroxyethyl (HE)-terminated PET fragment is released. Despite the remarkable performance of LCC-ICCG, the molecular origin of its superior activity remains insufficiently characterized. Gaining deeper mechanistic insights at the atomic level would provide constructive advice for the rational design and catalytic efficiency improvement of next-generation PET-hydrolyzing enzymes.
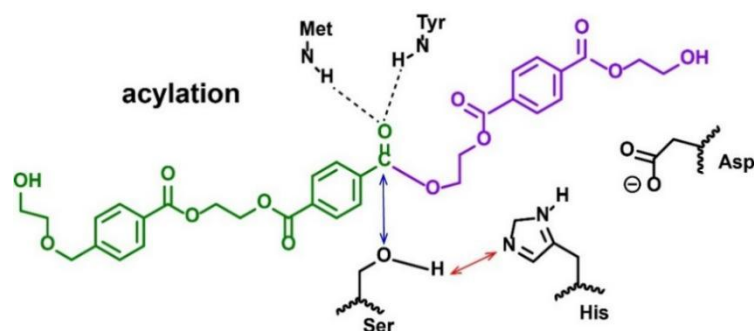
Scheme 1: Reaction mechanisms involved in catalytic degradation and systems involved in the QM calculation zone.

LCC-ICCG displayed superior performance over FAST-PETase and HotPETase under simulated industrial conditions (17). To probe the origin of its activity, PBS metrics were applied to MD trajectories. Catalytically productive geometries, defined by a Bürgi–Dunitz angle of 100–110° and a nucleophilic attack distance <3.5 Å, were sampled more frequently in LCC-ICCG (37.3%) compared to FAST-PETase (11.3%) or HotPETase (8.2%). Noncovalent interaction analyses revealed stronger hydrogen-bonding and dispersion contacts in LCC-ICCG, particularly involving residue V212, which stabilized both the catalytic triad and oxyanion hole (Figure 2d-f). Quantum topological analysis confirmed that bifurcated H-bonds between H242 and D237 strengthened proton transfer (–5.6 kcal/mol), surpassing values in FAST-PETase and HotPETase. These preorganized interactions explain the lower energy barriers observed experimentally (Figure 2i).
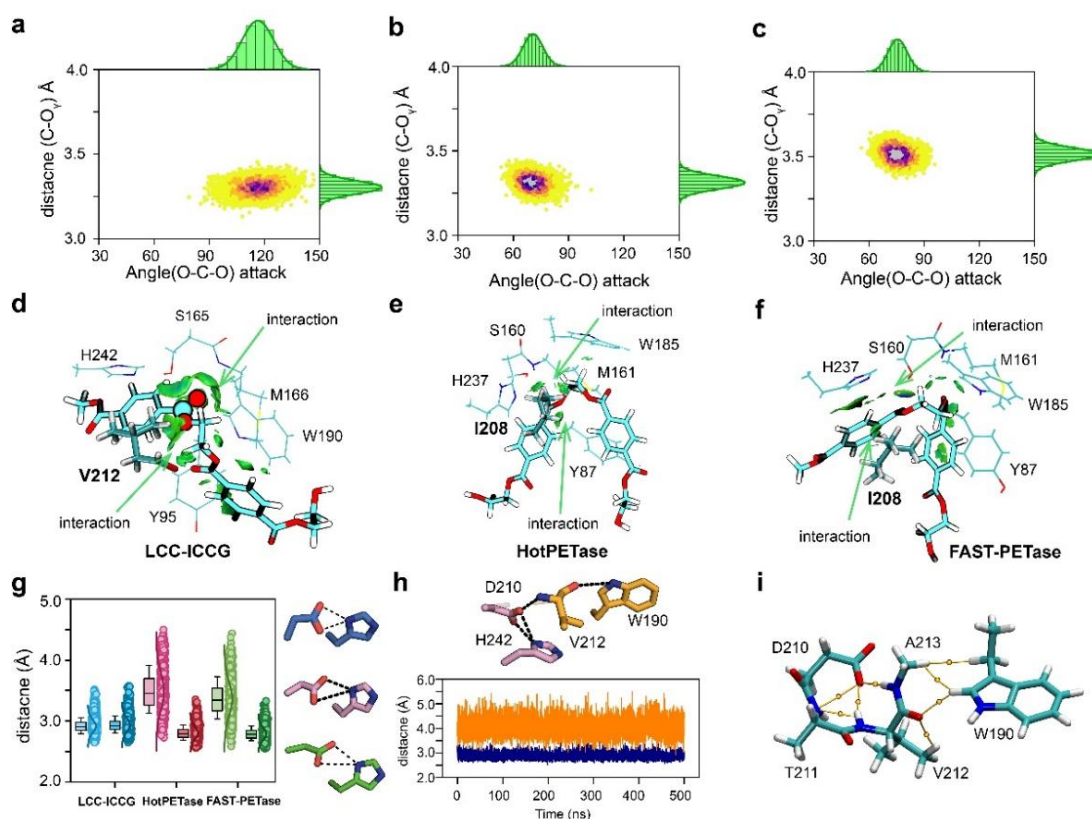

Figure 2: PBS analysis and non-covalent interaction analysis of enzyme. (a) Distribution of d(C-Oγ)

distances and Bürgi-Dunitz attack angles for LCC-ICCG, (b) HotPETase, and (c) FAST-PETase. (d) Non-covalent interaction analysis of LCC-ICCG, (e) HotPETase, and (f) FAST-PETase bound to the PET substrate. (g) Distance analysis of the hydrogen bonds between Asp and His in the catalytic triad. (h) Distance analysis (i) QTAIM analysis.

2.3 QM/MM Calculations Validate Energy Landscape

QM/MM cluster calculations of the acylation step showed that the calculated C–Oγ distances in the TSs were 1.97 Å (LCC-ICCG), 2.04 Å (HotPETase), and 2.02 Å (FAST-PETase). The corresponding barriers were 15.5, 19.3, and 20.4 kcal/mol, respectively, with the LCC-ICCG value aligning well with experimental kinetics (kcat = 0.7-4.8 s^{-1}; 13.5-18.0 kcal/mol, Eyring equation)(18). In contrast, HotPETase and FAST-PETase displayed higher barriers of 19.3 and 20.4 kcal/mol, respectively (Figure 3a-c). Distortion/interaction analysis revealed that LCC-ICCG benefits from reduced strain penalties and enhanced dispersion stabilization of the tetrahedral intermediate (Figure 3d). These results underscore the importance of PBS-derived conformational preorganization in lowering activation energy and accelerating PET depolymerization (Figure 3).
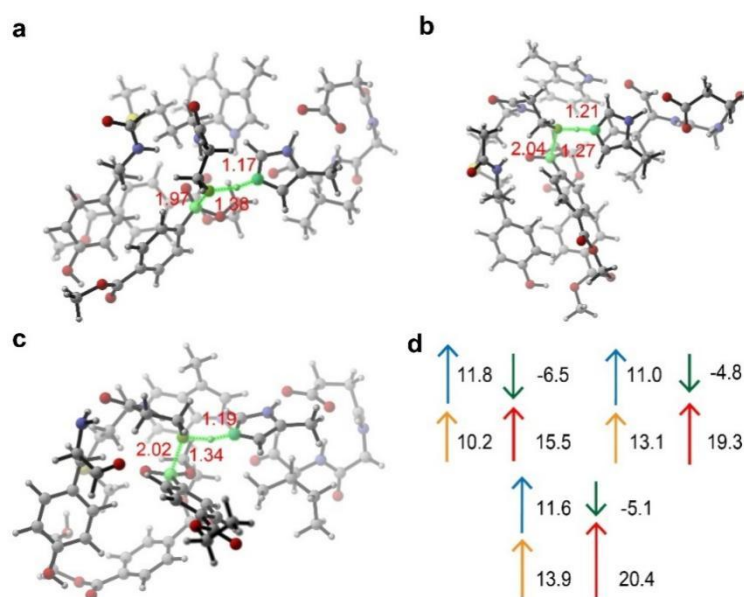

Figure 3: Computed mechanism of enzymatic PET biodegradation. The optimized transition structures (a)LCC-ICCG, (b)HotPETase and (c)FAST-PETase during acylation are highlighted. The distances are given in Angstrom. (d) The distortion/interaction activation strain analysis.

Multiscale QM/MM simulations further demonstrated that PET degradation proceeds through canonical acylation and deacylation steps. Statistical sampling indicated that water-mediated deacylation is the rate-determining step, consistent with kinetic measurements. While alternative Re-face attack pathways were energetically feasible in HiC, they were unfavorable in both LCC-ICCG and FAST-PETase, highlighting enzyme-specific mechanistic preferences (Figure 4).
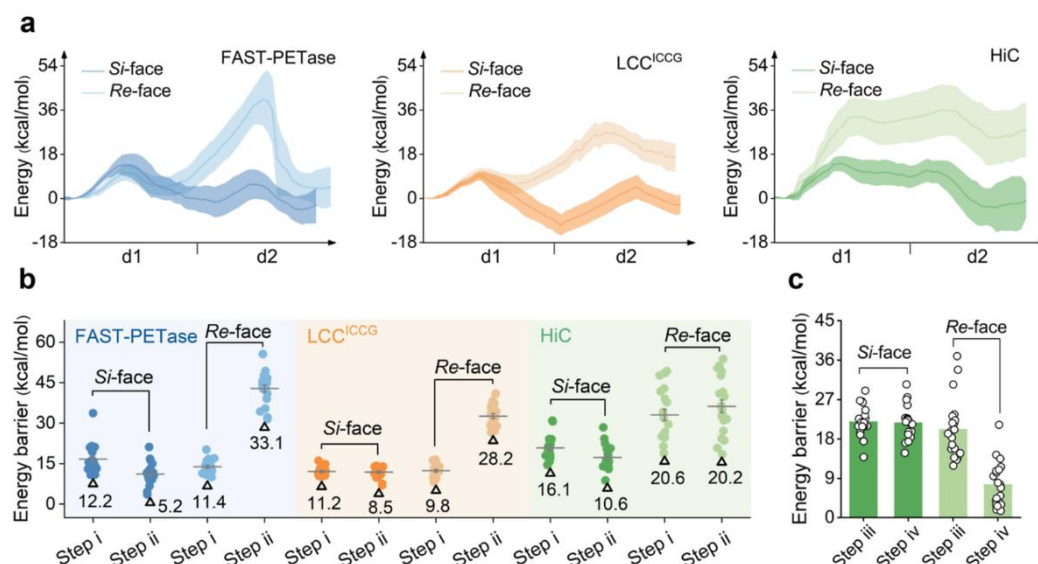
Figure 4: (a) Energy profile comparison for the acylation process. Energies of 20 independent enzyme conformations were calculated.

2.4 Directed Evolution Guided by Computational Predictions

Taking advantage of this intrinsic spectral feature, we designed a high-throughput assay in which the specific absorbance of reaction products served as a convenient readout, thereby facilitating the efficient discovery of LCC variants with superior PET-degrading activity(19). Virtual saturation mutagenesis coupled with affinity analysis yielded 21 candidate variants across six hotspots with reduced substrate affinity, which were subjected to activity validation. Screening revealed multiple variants retaining >75% of ICCG activity, seven of which outperformed ICCG against amorphous PET powder. The most active variant, H218Y, exhibited a 27% increase in depolymerization activity at 72 °C(Figure 5a). Previous studies reported that substitution of H218 with serine, together with F222I, improved activity below 60 °C but compromised performance at higher temperatures, underscoring the distinct advantage of H218Y at elevated conditions.

For the second cycle of protein engineering, the H218Y mutant was selected as the template, owing to its favorable catalytic performance and stability relative to other tested variants. Based on computational predictions, twelve candidate variants involving eight different residues were designed, most of which were expected to display reduced substrate affinity relative to H218Y. Experimental characterization revealed that ten of these variants, mainly arising from mutations at the S100, S101, N246, and S247, still maintained robust absorbance responses. Within this set, three double mutants—H218Y/S247E, H218Y/N248D, and H218Y/N248Q, demonstrated improved catalytic performance, with H218Y/N248D achieving the most pronounced effect, showing a 21% increase in activity compared with H218Y (Figure 5b).

Further evaluation of engineered variants revealed that LCC-ICCG-R2 and LCC-ICCG-R3 exhibited substantially enhanced catalytic efficiency, releasing 26.0 and 25.8 mM of depolymerization products within 6 h, respectively. By contrast, the parental ICCG enzyme generated only 18.5 mM

under the same conditions (Figure 5c). Product analysis confirmed that terephthalic acid (TPA) was the major depolymerization product, accompanied by smaller amounts of BHET and MHET. As a result, the predominant accumulation of TPA as the terminal product highlights both the enhanced catalytic performance and the practical potential of the rationally engineered variants.
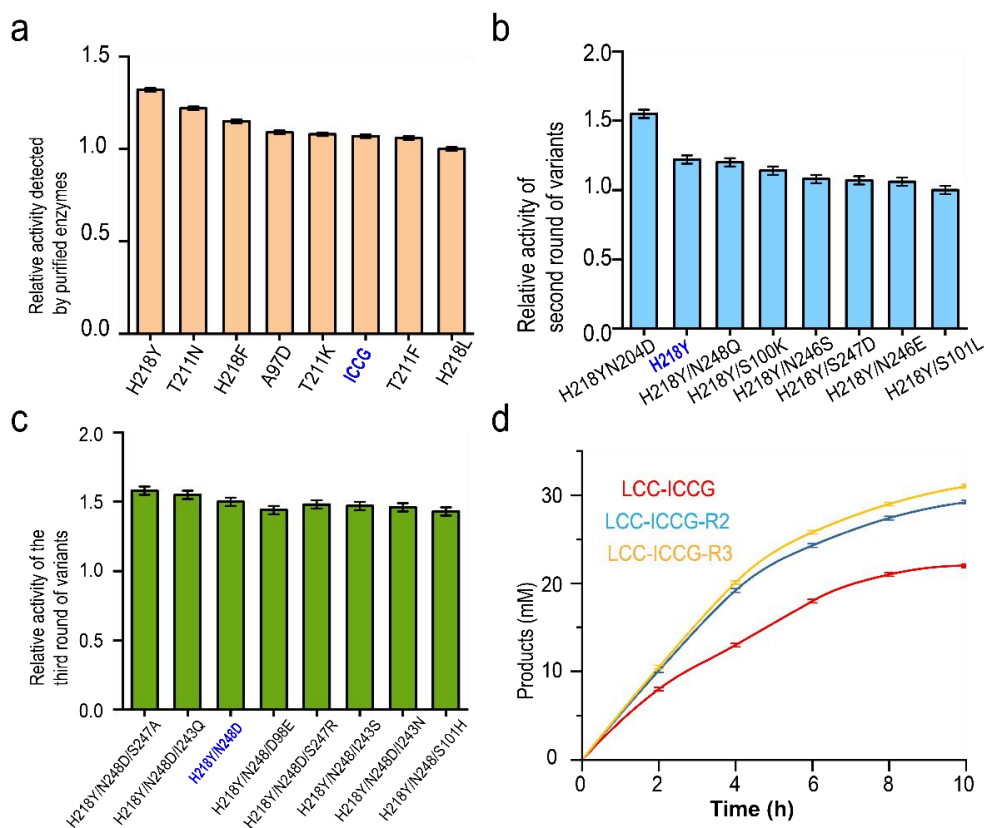

Figure 5: Relative PET depolymerization activities of variants exhibiting strong absorbance identified in the first (a), second (b), and third (c) rounds of engineering. Activities were determined by HPLC after depolymerization of amorphous PET powder at 72 °C for 5 h using purified enzymes, with data normalized to ICCG. (d) Time-dependent product release curves of ICCG, LCC-ICCG-R2, and LCC-ICCG-R3

Thermostability assays revealed Tm values of 95.3 and 94.7 °C for LCC-R2 and LCC-R3, respectively, slightly higher than ICCG, confirming that improved PET affinity did not compromise stability. Both variants exhibited optimal activity at 78 °C, surpassing the 75 °C optimum of ICCG. On amorphous PET film, LCC-ICCG-R2 and LCC-ICCG-R3 generated 53.8- and 51.2-mM products within 8 h, representing 2.7- and 2.5-fold increases relative to ICCG. Importantly, unlike other efficient hydrolases such as PHL-7, which predominantly accumulate MHET, the engineered variants yielded nearly complete depolymerization to TPA, highlighting their superior catalytic efficiency and product specificity.
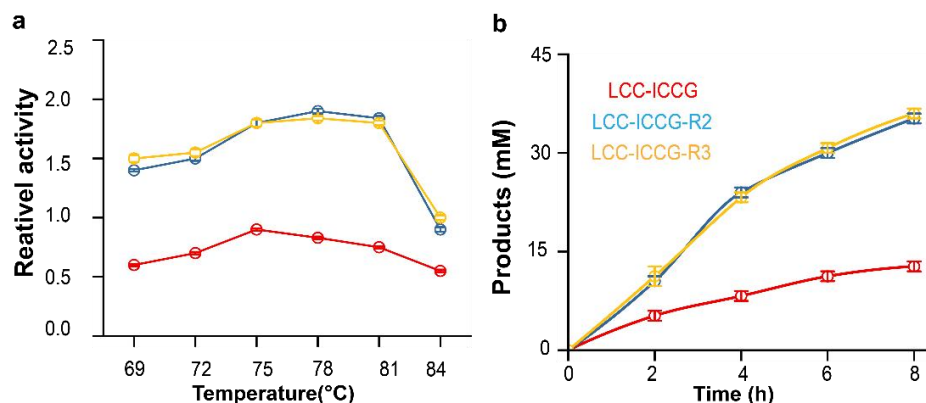
Figure 6: (a) Comparison of depolymerization activities of each variant toward amorphous PET powder at 69, 72, 75, 78, 81, and 84 °C for 2 h, with product concentrations determined by HPLC. Data are normalized to the highest ICCG activity (75 °C). (b) Depolymerization activity.

2.5 Extension to Copolyester Degradation

Candida antarctica lipase B (CALB) is a widely applied biocatalyst owing to its stability and broad substrate scope (20). To elucidate the depolymerization of PBTDP copolyesters, MD simulations were performed on PBTDP0 and PBTDP25. Transition state–like PBS conformations were defined from MD trajectories using frontier orbital analysis. Mechanistic insights revealed that the rate-limiting step is the nucleophilic attack of Ser105 on the substrate carbonyl. Scatterplot analysis showed that PBTDP25 preferentially adopted reactive PBS geometries, whereas PBTDP0 did not. Notably, 23.2% of PBTDP25 structures displayed productive PRS conformations. Residues W104 and A281 acted as a "claw" to capture pyrrolidone groups, maintaining short contacts (~3.5–4.0 Å) with the substrate, compared to 5.2–5.8 Å in PBTDP0(Figure 7c). IGMH and QTAIM analyses further confirmed stronger noncovalent interactions in PBTDP25–CALB complexes, rationalizing enhanced biodegradability (Figure 7d, e).

DFT cluster calculations for PBTDP25 indicated that two ester sites (E1, E2) exhibited high PRS populations (31.4% and 47.5%). The transition states during acylation reaction processed the activation barriers of 12.1 and 13.4 kcal/mol. These values are lower than reported CALB-mediated acylations with small molecules (13.9 kcal/mol), underscoring the favorable energetics of pyrrolidone-containing substrates (21), underscoring the favorable energetics of pyrrolidone-containing substrates. Collectively, these results highlight how pyrrolidone incorporation enhances CALB-catalyzed depolymerization, providing a molecular basis for the improved enzymatic degradability of PBTDP copolyesters.
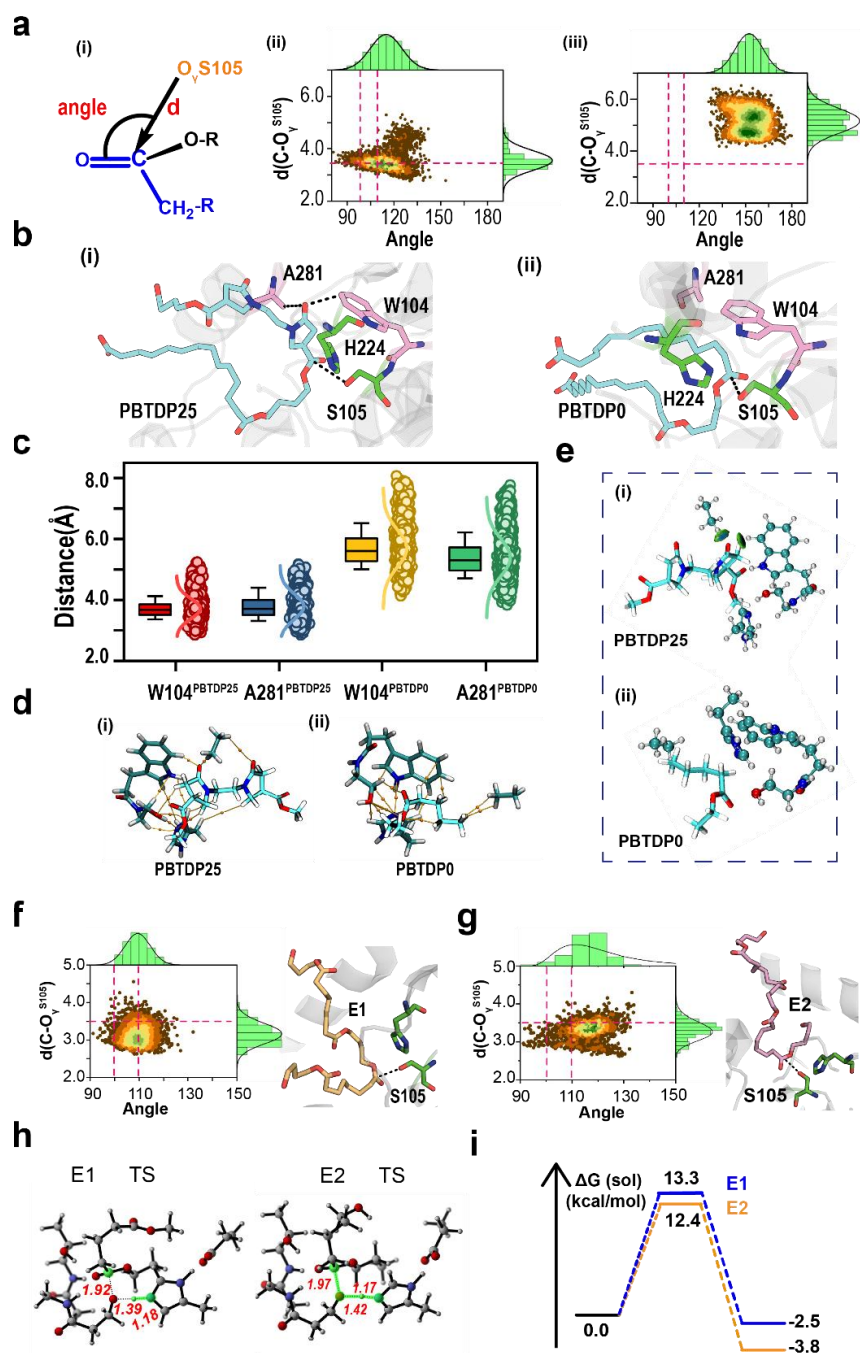
Figure 7: Comprehensive analysis of the catalytic mechanism (a) (i) A schematic representation illustrating the Bürgi–Dunitz angle (BD angle). (ii, iii) Two-dimensional distributions of nucleophilic attack distance $d(C-O\gamma^{S105})$ and BD angle obtained from MD simulations. (b) Representative binding conformations derived from clustering of MD trajectories for (i) PBTDP25–CALB and (ii) PBTDP0–CALB complexes. (c) Quantification of NCI by monitoring the sampling distances between substrate atoms and residue W104 across MD simulations. (d) Topological analysis of PBTDP-CALB complex via popular QTAIM framework. (e) IGMH analysis. (f, g) PBS analyses of (f) E1 and (g)E2 bound with CALB during MD simulations. (h) Optimized transition-state (TS) structures of the acylation step. Key distances are indicated in Å. (i) Free energy profiles of the enzymatic degradation pathway.

2.6 Selective Enzymatic Recycling from Mixed Plastic Waste

Hydrolysates obtained from PBTDP depolymerization can be directly recycled as high-purity monomers, offering an energy-efficient and environmentally friendly route to polymer re-synthesis. Unlike conventional recycling methods that suffer from property deterioration, this approach supports a true circular economy. A major challenge in plastic recycling is selective depolymerization from mixed waste streams. Here, we show that PBTDP20 can be selectively degraded in mixtures with PP, PVC, and PET. Upon incubation with CALB (240 μg/mL, PBS pH 7.4, 37 °C), only PBTDP20 films underwent rapid enzymatic hydrolysis, while commodity plastics remained intact. After 2 days, PBTDP20 fragmented, and the long-chain diacid TDA precipitated as a fine powder, yielding 92% recovery, while pyrrolidone-based oligomers persisted in solution.

This selectivity arises from the orthogonal reactivity of pyrrolidone diacid units, combined with the intrinsic stability of PP, PVC, and PET under mild conditions. Compared to previous enzymatic recycling systems, our use of unmodified, commercially available CALB achieved recovery yields surpassing most wild-type hydrolases and approaching engineered enzymes such as TurboPETase, without requiring protein engineering. Moreover, the process was conducted entirely in aqueous medium at 37 °C, avoiding toxic solvents and reducing energy demand. CALB retained activity after storage at 37 °C for 10 days, and its known stability in immobilized formulations suggests further opportunities for scalable, cost-effective enzymatic recycling.
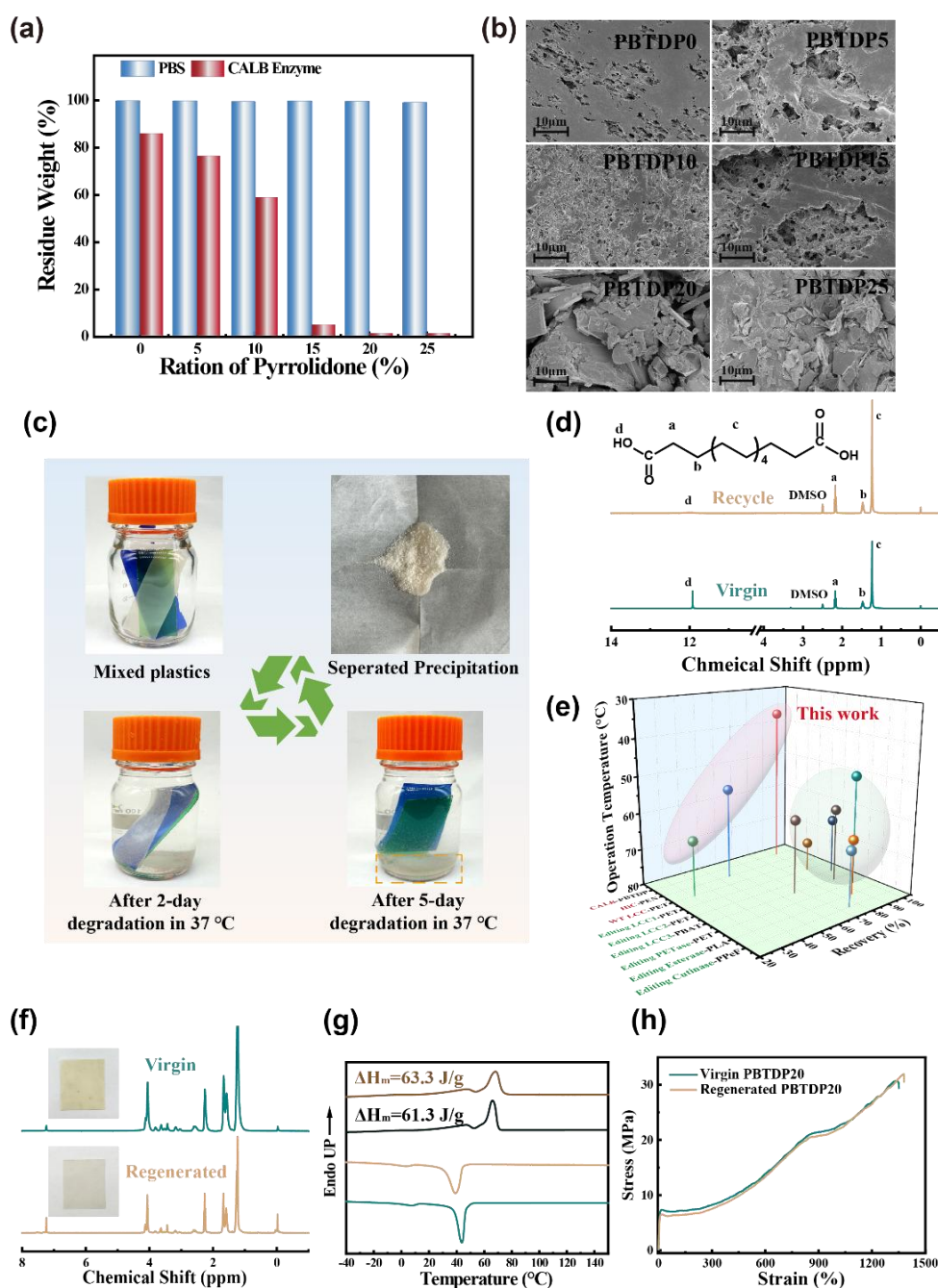
Figure 8: (a) Mass loss of PBTDP20/25 after 10 days: complete degradation under CALB catalysis. (b) SEM: porous, fractured surfaces after enzymatic attack. (c) Enzymatic depolymerization and chemical recycling of PBTDP20 carried out in the presence of mixed plastic waste streams containing PET, PP, and PVC. The results demonstrate the selectivity of the process, highlighting the efficient breakdown of PBTDP20 even in a heterogeneous waste environment. (d) 1H NMR spectra comparison between virgin and recycled 2,5-thiophenedicarboxylic acid (TDA). (e) Comparison of monomer recovery efficiency: this work's CALB system vs. wild-type and engineered enzyme systems. (f) ^{1}H NMR: virgin vs. regenerated PBTDP20. (g) DSC: regenerated polymer exhibits similar crystallinity to virgin. (h) Mechanical performance: regenerated retains or surpasses virgin polymer.

3. Discussion

Overall, the PBS model provided a predictive framework for designing high-activity PET hydrolases. Computationally guided mutations yielded variants with markedly improved depolymerization activity and industrial robustness. Extension to synthetic copolyesters and selective recycling experiments demonstrates the broader applicability of the strategy. By integrating theory, simulation, and directed evolution, this work establishes a systematic route toward biocatalyst engineering for plastic degradation.

Under our conditions, the conformational population of a single enzyme variant can be obtained within 15 minutes using one GPU (NVIDIA GeForce RTX 3090) and one CPU. In contrast, manual modeling of a single variant requires nearly 50 minutes due to structural manipulations, file preparation, and simulation runtime. More importantly, experimental characterization of one enzyme variant—including mutagenesis, sequencing, transformation, expression, purification, and activity assays—typically takes about seven days. This highlights the time-saving advantage of PBS, particularly given the inherent limitations of experimental throughput.

Furthermore, when computational resources are ample, the efficiency of NAC-based evaluation scales favorably with larger mutational spaces, offering the potential to screen hundreds of thousands or even millions of variants. This acceleration can substantially lower the cost of experimental screening while promoting the identification of mutations that improve catalytic activity. Nevertheless, we do not overstate the current findings, as NAC-based ranking may not fully correlate with experimental outcomes and does not account for factors such as expression level or solubility. In addition, MD sampling may become trapped in local minima or provide insufficient coverage of accessible conformational space, which requires careful consideration in future refinements.

The PBS framework was further applied to dissect enzyme–substrate recognition of *Candida antarctica* lipase B (CALB) toward bio-based pyrrolidone-containing polyesters (PBTDPs). Incorporation of N,N′-dimethylene-bis(pyrrolidone-4-carboxylic acid) into polyethylene-like backbones introduced polarity, hydrophilicity, and specific recognition motifs. Combined MD and PBS analyses revealed that PBTDP25 sampled a substantially higher fraction of catalytically competent geometries compared to PBTDP0, consistent with experimental results showing complete disintegration and 92% monomer recovery within 2–10 days at 37 °C. Complementary DFT calculations indicated that PBS-guided designs lowered hydrolytic activation barriers by ~7 kcal/mol, thereby rationalizing the mild-condition degradability. Together, this closed-loop integration of computation, design, and experimental validation provides a generalizable paradigm for engineering high-performance yet recyclable polymers.

4. Computational Details and Methods
4.1 Computational Design of PBS Conformations
We defined PBS conformations as low-energy structural states that approximate transition-state geometries in catalytic or binding processes. Conformations were categorized as active PBSs if the distance and angle approximated the transition-state geometry. Conformational populations were

evaluated using MD simulations, and PBS frequencies were quantified across trajectories. The conformational landscape was first explored using the CREST software (part of the XTB package) at the GFN2-xTB level (22). Then, the most stable conformers obtained were further refined through DFT calculations. All DFT calculations in this study were performed in the Gaussian 16 quantum chemistry software package, using the dispersion-corrected ωB97X-D functional (a dual-hybrid functional optimized within the GFN-xTB framework, particularly suitable for medium-sized molecular systems with weak interactions) combined with the 6-31+G(d,p) basis set(23). To simulate the effects of an aqueous environment on the molecular electronic structure, the SMD implicit solvation model was incorporated into all small molecule optimization and property calculations. We also performed the frequency calculations to confirm whether the structure is at a local energy minimum (no imaginary frequencies or only low-frequency imaginary and calculate the key thermodynamic data for Gibbs free energy (24).

4.2 System Preparation

Through AMBER 2022 package, the system was subjected to extensive MD simulations (25). We used cpptraj module in AMBER software to analysis the trajectory, and generating the values of like root-mean-square deviations (RMSD) values (26). The enzyme-polymer complex was generated using AutoDock Vina v1.2.0 (27). At the HF/6-31G(d) level, the force field parameters for the polymers were derived by calculating the electrostatic potential. The resulting charge distributions were then subjected to a two-stage restrained ESP (RESP) fitting procedure within the Antechamber module, yielding bonded and van der Waals radii parameters (28). The protonation states were calculated to accurately represent the electrostatic properties of the protein. These states were predicted via the H++ server (29). Protein atoms were represented with the ff19SB force field. To begin system construction, each complex was placed in an octahedral TIP3P water box, maintaining a minimum distance of 12 Å. Subsequently, we neutralized the system by adding Na^+ counterions.

4.3 Molecular Dynamics Simulations

Prior to production simulations, atomic clashes were eliminated through a two-step energy minimization procedure. The first step is to optimize the positions of water molecules and then relax the entire solvated system. After the minimization, the systems were then heated from 0 K to 300 K over 50 ps in the NVT ensemble, with temperature regulation achieved through a Langevin thermostat. This was followed by an equilibration phase under the NPT ensemble for 100 ps, allowing the systems to attain appropriate bulk density. To improve sampling robustness, ten independent replica simulations were conducted for initial 10 ns production MD run. From these, three replicas that displayed stable hydrogen-bonding networks were selected and extended to 100 ns each. Among these, the trajectory that best represented key reactive conformational states was further extended to 500 ns for enhanced conformational sampling. In all simulations, the Particle Mesh Ewald (PME) method was utilized to accurately treat long-range electrostatic interactions, thereby ensuring a reliable

representation of the system's electrostatic environment (30). We carried out binding energy calculation via MM/GBSA method, in which frames were uniformly sampled from the final 200 ns of the 500 ns production run, resulting in 3000 snapshots per condition for subsequent analysis (31).

We analyzed the noncovalent interactions through the reduced density gradient (RDG) method (32). Interaction type and strength were discriminated by mapping the function sign(λ_2)ρ onto the RDG isosurfaces. Negative sign(λ_2)ρ values indicated attractive interactions (e.g., hydrogen bonding interaction), whereas positive values corresponded to steric repulsion. The approach was complemented by the IGMH method that enable broader characterization of noncovalent contacts across molecular interfaces (33).

4.4 Materials and Experimental Procedures

Unless otherwise specified, all chemicals were purchased from recognized suppliers and applied directly without further purification. Representative examples include 1,4-butanediol (1,4-BDO, 99%) and ethylenediamine (EDA, 99%). These compounds served as essential building blocks for the preparation of polymeric substrates and model compounds used in the enzymatic degradation study. Catalysts and additives included titanium (IV) butoxide (TBT, 99%), frequently utilized as a Lewis acid catalyst in esterification and polycondensation, and antimony trioxide (Sb$_2$O$_3$, 99.5%), which was employed as a co-catalyst to promote polycondensation efficiency and thermal stability. Functional monomers such as itaconic acid (IA, 99%) were incorporated as renewable, bio-based dicarboxylic acids to provide reactive sites and modulate polymer chain architecture, thereby facilitating enzymatic accessibility during subsequent degradation processes. The organic solvents used in the experiments (chloroform, tetrachloroethane, and o-chlorophenol) were all obtained from Sinopharm Chemical Reagent Co., Ltd. (Shanghai, China). Candida antarctica lipase B (CALB, with an enzyme activity content of approximately 6%) was provided by Novozymes Biotech (China) Co., Ltd. (Beijing, China).

BHET and TPA were purchased from Sigma-Aldrich, and MHET was obtained from Aladdin (Shanghai, China). All other chemicals were of the highest purity and supplied by Sigma-Aldrich. Briefly, 2 g PET was dissolved in 20 mL trifluoroacetic acid (TFA, 90% v/v) at 50 °C under stirring for 2 h. The solution was then precipitated by slowly adding 20 mL diluted TFA (20% v/v) under vigorous stirring for another 2 h. After centrifugation (2500 g, 1 h), the supernatant was discarded, and the pellet was resuspended in 200 mL 0.5% sodium dodecyl sulfate (SDS) solution, followed by ultrasonication for 30 min to homogenize the particles.

4.5 Gene Construction and Mutagenesis

The codon-optimized gene encoding the LCC variant ICCG was synthesized by a commercial provider (e.g., GenScript, Nanjing, China) and subcloned into the pET26b(+) expression plasmid between the Nde I (5′) and Xho I (3′) restriction sites, incorporating a C-terminal His6-tag. Site-directed mutagenesis was carried out using PCR with Phusion High-Fidelity DNA polymerase

(Thermo Fisher Scientific, USA), and primers were designed to introduce the required substitutions with overlapping regions for recombination. PCR products were digested with Dpn I to remove the parental template, purified, and assembled into circular plasmids.

4.6 Protein Expression and Purification

Recombinant LCC variants were expressed in *E. coli* BL21 (DE3). Expression was induced by the addition of 0.5 mM IPTG, followed by incubation at 37 °C for 16 h. Cells were harvested by centrifugation (8000 rpm, 10 min), and the soluble fraction was clarified by filtration through a 0.45 μm membrane. Proteins were purified via Ni-NTA affinity chromatography (Cytiva, Sweden). After washing with buffer containing 20 mM Tris-HCl (pH 8.0), 300 mM NaCl, and 20 mM imidazole, the target protein was eluted with 250 mM imidazole. The eluate was concentrated and buffer-exchanged into storage buffer (20 mM Tris-HCl, pH 8.0, 100 mM NaCl) using centrifugal ultrafiltration devices (10 kDa cutoff, Sartorius, Germany).

4.7 Depolymerization of Post-Consumer PET in Bioreactor

Post-consumer PET powder (10 g) was suspended in 0.1 M phosphate buffer (pH 8.5, final volume 40 mL) in a 100 mL round-bottom centrifuge tube and pre-incubated at the indicated temperature for 15 min with agitation at 300 rpm to ensure homogeneity. Purified enzyme (30 mg) was then added, and reactions were conducted in a parallel bioreactor system equipped with automated pH control. The pH was maintained at 8.5 using NaOH titration, and NaOH consumption was used to calculate TPA release (2 mol NaOH neutralizes 1 mol TPA), thereby determining PET depolymerization efficiency. Reaction products were analyzed by HPLC to quantify the composition of depolymerization products.

Reference

1. A. Chamas, H. Moon, J. Zheng, Y. Qiu, et al. Degradation Rates of Plastics in the Environment. *ACS Sustainable Chemistry & Engineering* 8, 3494–3511. (2020).
   DOI: https://doi.org/10.1021/acssuschemeng.9b06635

2. U. T. Bornscheuer. Feeding on Plastic. *Science* 351, 1154–1155. (2016).
   DOI: https://doi.org/10.1126/science.aaf2853

3. S. Kakadellis, & G. Rosetto. Achieving a Circular Bioeconomy for Plastics. *Science* 373, 49–50. (2021).
   DOI: https://doi.org/10.1126/science.abj3476

4. L. D. Ellis, N. A. Rorrer, K. P. Sullivan, et al. Chemical and Biological Catalysis for Plastics Recycling and Upcycling. *Nature Catalysis* 4, 539–556. (2021).
   DOI: https://doi.org/articles/s41929-021-00648-4

5. J. M. Garcia, M. L. Robertson, The Future of Plastics Recycling. *Science* 358, 870-872. (2017).
   DOI: https://doi.org/10.1126/science.aaq0324

6. E. Erickson, J. E. Gado, L. Avilán, F. Bratti, et al. Sourcing Thermotolerant Poly(ethylene terephthalate) Hydrolase Scaffolds from Natural Diversity. *Nature Communications* 13, 7850. (2022).
   DOI: https://doi.org/10.1038/s41467-022-35237-x

7. R. Wei, G. Weber, L. M. Blank, U. T. Bornscheuer, Process Insights for Harnessing Biotechnology for Plastic Depolymerization. *Nature Chemical Engineering* 2, 110–117. (2025).
   DOI: https://doi.org/10.1038/s44286-024-00171-w

8. H. Hong, D. Ki, H. Seo, J. Park, et al. Discovery and Rational Engineering of PET Hydrolase with Both Mesophilic and Thermophilic PET Hydrolase Properties. *Nature Communications* 14, 4556. (2023).
   DOI: https://doi.org/10.1038/s41467-023-40233-w

9. L. Shi, P. Liu, Z. Tan, W. Zhao, et al. Complete Depolymerization of PET Wastes by an Evolved PET Hydrolase from Directed Evolution. *Angewandte Chemie* 62, e202218390. (2023).
   DOI: https://doi.org/10.1002/anie.202218390

10. V. Tournier, S. Duquesne, F. Guillamot, H. Cramail, et al. Enzymes' Power for Plastics Degradation. *Chemical Reviews* 123, 5612–5701 (2023).
    DOI: https://doi.org/10.1021/acs.chemrev.2c00644

11. S. Wu, R. Snajdrova, J. C Moore, K. Baldenius, U. T Bornscheuer. Biocatalysis: Enzymatic Synthesis for Industrial Applications. *Angewandte Chemie International Edition* 60, 88–119. (2021).
    DOI: https://doi.org/10.1002/anie.202006648

12. L. Jiang, E. A. Althoff, F. R. Clemente, L. Doyle, et al. De Novo Computational Design of Retro-Aldol Enzymes. *Science* 319, 1387–1391, (2008).
    DOI: https://doi.org/10.1126/science.1152692

13. P. N. Devine, R. M. Howard, R. Kumar, M. P. Thompson, et al. Extending the Application of Biocatalysis to Meet the Challenges of Drug Development. *Nature Reviews Chemistry* 2, 409–421, (2018).
   DOI: https://doi.org/10.1038/s41570-018-0055-1

14. B. Hauer, Embracing Nature's Catalysts: A Viewpoint on the Future of Biocatalysis. *ACS Catalysis* 10, 15, 8418–27, (2020).
   DOI: https://doi.org/10.1021/acscatal.0c01708

15. C. K. Winkler, J. H. Schrittwieser, W. Kroutil, Power of Biocatalysis for Organic Synthesis. *ACS Central Science* 7, 55–71, (2021).
   DOI: https://doi.org/10.1021/acscentsci.0c01496

16. E. Bell, R. Smithson, S.Kilbride, et al. Directed Evolution of An Efficient and Thermostable Pet Depolymerase. *Nature Catalysis* 5, 673-681. (2022).
   DOI: https://doi.org/10.1038/s41929-022-00821-3

17. G. Arnal, J. Anglade, S.Gavalda, et al. Assessment of Four Engineered PET Degrading Enzymes Considering Large-Scale Industrial Applications. *ACS Catalysis* 13,13156-13166. (2023).
   DOI: https://doi.org/10.1021/acscatal.3c02922

18. L. Pfaff, J. Gao, Z. Li, et al. Multiple Substrate Binding Mode-Guided Engineering of a Thermophilic Pet Hydrolase. *ACS Catalysis* 12, 9790-9800. (2022).
   DOI: https://doi.org/10.1021/acscatal.2c02275

19. C.C. Chen, X. Han, X. Li, et al. General Features to Enhance Enzymatic Activity of Poly (Ethylene Terephthalate) Hydrolysis. *Nature Catalysis 4,* 425-430. (2021).
   DOI: https://doi.org/10.1038/s41929-021-00616-y

20. S. Schubert, K. Schaller, J. A. Baath, et al. Pathways for the Enzymatic Degradation of Poly (Ethylene Terephthalate): What Characterizes an Efficient PET-Hydrolase. *ChemBioChem* 24, e202200516. (2023).
   DOI: https://doi.org/10.1002/cbic.202200516

21. M.A. Galmes, E. García-Junceda, K. Swiderek, et al. Exploring the Origin of Amidase Substrate Promiscuity In Calb By a Computational Approach. *ACS Catalysis* 10, 1938-1946. (2019).
   DOI: https://doi.org/10.1021/acscatal.9b04002

22. P. Pracht, F.Bohle, S. Grimme. Automated Exploration of the Low-Energy Chemical Space with Fast Quantum Chemical Methods. *Physical   Chemistry Chemical Physics* 22, 7169-7192. (2020).
   DOI: https://doi.org/10.1039/C9CP06869D

23. B. S. Schreib, & E. M. Carreira. Palladium-Catalyzed Regioselective C–H Iodination of Unactivated Alkenes. *Journal of the American Chemical   Society* 141, 8758–8763. (2019).
   DOI: https://doi.org/10.1021/jacs.9b03998

24. S. Maeda, Y. Harabuchi, Y. Ono, et al. Intrinsic Reaction Coordinate: Calculation, Bifurcation, and Automated Search. *International Journal of Quantum Chemistry* 115, 258-269. (2015)
   DOI: https://doi.org/10.1002/qua.24757

25. R. Salomon-Ferrer, A. W. Gotz, D. Poole, et al. Routine Microsecond Molecular Dynamics Simulations with AMBER on GPUs. 2. Explicit Solvent Particle Mesh Ewald. *Journal of Chemical Theory and Computation* 9, 3878−3888. (2013).

DOI: https://doi.org/10.1021/ct400314y

26. D. R. Roe, & T. E. Cheatham III. PTRAJ and CPPTRAJ: Software for Processing and Analysis of Molecular Dynamics Trajectory Data. *Journal of Chemical Theory and Computation* 9, 3084-3095. (2013).
    DOI: https://doi.org/10.1021/ct400341p

27. O. Trott, A. J. Olson. AutoDock Vina: Improving the Speed and Accuracy of Docking With a New Scoring Function, Efficient Optimization and Multithreading. *Journal of computational chemistry* 31, 455-461. (2010).
    DOI:https://doi.org/10.1002/jcc.21334

28. T. Shi, L. Liu, W. Tao, et al. Theoretical Studies on the Catalytic Mechanism and Substrate Diversity for Macrocyclization of Pikromycin Thioesterase. *ACS Catalysis* 8, 4323-4332. (2018).
    DOI: https://doi.org/10.1021/acscatal.8b01156

29. Anandakrishnan, R.; Aguilar, B.; Onufriev, A. V. H++ 3.0: automating pK prediction and the preparation of biomolecular structures for atomistic   molecular modeling and simulation. *Nucleic Acids Research* 40, W537−541. (2012).
    DOI: https://doi.org/10.1093/nar/gks375

30.C. Sagui, L. G. Pedersen, T. A. Darden. Towards an Accurate Representation of Electrostatics in Classical Force Fields: Efficient Implementation of Multipolar Interactions in Biomolecular Simulations. *The Journal of Chemical Physics* 120, 73−87. (2004).
    DOI:https://doi.org/10.1063/1.1630791

31. B. R. Miller, T. D. McGee, J. M. Swails, et al. MMPBSA. Py: An Efficient Program for End-State Free Energy Calculations. *Journal of Chemical Theory and Computation* 8, 3314−3321. (2012).
    DOI: https://doi.org/10.1021/ct300418h

32. E. R. Johnson, S. Keinan, P. Mori-Sanchez. Revealing Noncovalent   Interactions. *Journal of the American Chemical Society* 132, 6498–6506. (2010).
    DOI: https://doi.org/10.1021/ja100936w

33. T. Lu, & Q. Chen. Independent Gradient Model Based on Hirshfeld Partition: A New Method for Visual Study of Interactions in Chemical Systems. *Journal of Computational Chemistry* 43, 539−555. (2022).
    DOI: https://doi.org/10.1002/jcc.26812